PROCEEDINGS OF SPIE

SPIEDigitalLibrary.org/conference-proceedings-of-spie

Aspera: the UV SmallSat telescope to detect and map the warm-hot gas phase in nearby galaxy halos

Chung, Haeun, Vargas, Carlos, Hamden, Erika, McMahon, Tom, Gonzales, Kerry, et al.

Haeun Chung, Carlos J. Vargas, Erika Hamden, Tom McMahon, Kerry Gonzales, Aafaque R. Khan, Simran Agarwal, Hop Bailey, Peter Behroozi, Trenton Brendel, Heejoo Choi, Tom Connors, Lauren Corlies, Jason Corliss, Ralf-Jürgen Dettmar, David Dolana, Ewan S. Douglas, John Guzman, Dave Hamara, Walt Harris, Karl Harshman, Carl Hergenrother, Keri Hoadley, John Kidd, Daewook Kim, Jessica S. Li, Manny Montoya, Corwynn Sauve, David Schiminovich, Sanford Selznick, Oswald Siegmund, Michael Ward, Ellie M. Wolcott, Dennis Zaritsky, "Aspera: the UV SmallSat telescope to detect and map the warm-hot gas phase in nearby galaxy halos," Proc. SPIE 11819, UV/Optical/IR Space Telescopes and Instruments: Innovative Technologies and Concepts X, 1181903 (20 August 2021); doi: 10.1117/12.2593001

SPIE.

Event: SPIE Optical Engineering + Applications, 2021, San Diego, California, United States

Aspera: The UV SmallSat telescope to detect and map the warm-hot gas phase in nearby galaxy halos

Haeun Chung[a], Carlos J. Vargas[a], Erika Hamden[a], Tom McMahon[a], Kerry Gonzales[a], Aafaque R. Khan[a,b], Simran Agarwal[b], Hop Bailey[c], Peter Behroozi[a], Trenton Brendel[b], Heejoo Choi[b,j], Tom Connors[a], Lauren Corlies[d], Jason Corliss[c], Ralf-Jürgen Dettmar[e], David Dolana[a], Ewan S. Douglas[a], John Guzman[a], Dave Hamara[c], Walt Harris[c], Karl Harshman[c], Carl Hergenrother[f], Keri Hoadley[g,k], John Kidd[f], Daewook Kim[a,b,j], Jessica S. Li[a,l], Manny Montoya[a], Corwynn Sauve[a], David Schiminovich[h], Sanford Selznick[f], Oswald Siegmund[i], Michael Ward[a], Ellie M. Wolcott[a], and Dennis Zaritsky[a]

[a]Steward Observatory, University of Arizona, 933 N. Cherry Ave., Tucson, AZ 85721, USA
[b]Wyant College of Optical Sciences, University of Arizona, 1630 E. University Blvd., Tucson, AZ 85721, USA
[c]Lunar and Planetary Laboratory, University of Arizona, 1629 E University Blvd., Tucson, AZ 85721, USA
[d]AURA/Vera C. Rubin Observatory, 950 N. Cherry Ave., Tucson, AZ 85719, USA
[e]Ruhr University Bochum, Faculty of Physics and Astronomy, Astronomical Institute, 44780 Bochum, Germany
[f]Ascending Node Technologies, LLC.
[g]The University of Iowa, Dept. of Physics & Astronomy, Van Allen Hall, Iowa City, IA 52242, USA
[h]Columbia University, 550 W. 120th Street, New York, NY 10027, USA
[i]Sensor Sciences LLC, 3333 Vincent Road, Suite 103, Pleasant Hill, CA 94523, USA
[j]Large Binocular Telescope Observatory, University of Arizona, 933 N Cherry Avenue, Tucson, AZ 85721, USA
[k]California Institute of Technology, Dept. of Physics, Mathematics, and Astronomy, Cahill Center for Astronomy & Astrophysics, Pasadena, CA 91125, USA
[l]Department of Physics, University of Arizona, 1118 E. Fourth Street, Tucson, AZ 85721

ABSTRACT

Aspera is an extreme-UV (EUV) Astrophysics small satellite telescope designed to map the warm-hot phase coronal gas around nearby galaxy halos. Theory suggests that this gas is a significant fraction of a galaxy's halo mass and plays a critical role in its evolution, but its exact role is poorly understood. *Aspera* observes this warm-hot phase gas via O VI emission at 1032 Å using four parallel Rowland-Circle-like spectrograph channels in a single payload. *Aspera*'s robust-and-simple design is inspired by the FUSE spectrograph, but with smaller, four 6.2 cm × 3.7 cm, off-axis parabolic primary mirrors. *Aspera* is expected to achieve a sensitivity of 4.3×10^{-19} erg/s/cm^2/arcsec^2 for diffuse O VI line emission. This superb sensitivity is enabled by technological advancements over the last decade in UV coatings, gratings, and detectors. Here we present the overall payload design of the *Aspera* telescope and its expected performance. *Aspera* is funded by the inaugural 2020 NASA Astrophysics Pioneers program, with a projected launch in late 2024.

Keywords: UV, Spectrograph, O VI Emission, NASA Astrophysics Pioneers, Circumgalactic Medium, Small Satellite, Space Telescope, Micro-Channel Plate

Further author information: (Send correspondence to H. Chung)
H. Chung: E-mail: haeunchung@arizona.edu,
C. J. Vargas: E-mail: cjvargas@arizona.edu

UV/Optical/IR Space Telescopes and Instruments: Innovative Technologies and Concepts X, edited by Allison A. Barto, James B. Breckinridge, H. Philip Stahl, Proc. of SPIE Vol. 11819, 1181903 · © 2021 SPIE · CCC code: 0277-786X/21/$21 · doi: 10.1117/12.2593001

1. INTRODUCTION

Aspera is a UV SmallSat mission designed to map the warm-hot phase coronal gas in nearby galaxy halos for the first time. *Aspera* was selected as part of NASA's first Astrophysics *Pioneers* missions in January 2021 and is currently in its Concept Study phase. Dr. Carlos Vargas (University of Arizona) is the Principal Investigator of the mission.

Different phases of the circumgalactic medium (CGM) constantly flow in and out of galaxies, creating a complex environment around the galaxy. This gas interacts with pristine material from farther out in the intergalactic medium and metal-rich material blown out of the inner galaxy. The CGM is expected to be multi-phase, and the warm-hot phase (T $\sim 10^5$ to 10^6 K), has only been observed under limited conditions (e.g., single sight-lines or at redshifts greater than 1).[1–3] This warm-hot phase gas contains more mass than the stars within the parent galaxy and could be the dominant baryonic component of galaxies.[3] Despite its importance to the formation and evolution of galaxies, its mass, kinematics, and spatial distribution are poorly constrained. This ignorance is mainly due to the fact that its brightest emission tracer, the Oxygen VI (O VI) doublet (λ = 1032, 1036 Å), is extremely faint, distributed over very wide angular areas on the sky, emitted in the extreme UV (EUV), and is challenging to observe with the currently available instruments, including the UV instruments currently aboard the Hubble Space Telescope (HST). *Aspera* is specially designed to detect this warm-hot phase of galactic CGMs.

To detect and map the warm-hot phase gas in the nearby galaxy halos, *Aspera* was designed and proposed to the 2020 NASA Astrophysics Pioneers Announcement of Opportunity (AO). *Aspera* observes the O VI 1032 Å emission line, a major tracer of the warm-hot phase CGM, using four parallel channels of Rowland-Circle-like spectrographs in a single payload. Each spectrograph contains a 6.2 cm × 3.7 cm off-axis parabola (OAP) primary mirror and a toroidal diffraction grating. The spectrograph design is inspired by the Medium-size Explorer class (MIDEX) mission, the Far Ultraviolet Spectroscopic Explorer (FUSE), which operated in a similar wavelength range but with a larger telescope aperture (4 channels, 39 cm × 35 cm primary) and multiple slit sizes. FUSE was designed to have a high point source spectral resolution (R>10,000), but this high resolution made FUSE to be less sensitive to the diffuse sources. Though in a fraction of mass, size, and cost cap of FUSE, *Aspera* will achieve equal or better diffuse source sensitivity than FUSE, by having lower spectral resolution (R>1,500) with the improved throughput of the grating and the detector. *Aspera*'s optical system is optimally designed for faint, diffuse source detection with wide field of view (60′). Ascending Node Technologies is the mission design partner of *Aspera*. *Aspera*, currently in the conceptual design phase and in the process of finalizing a spacecraft vendor, is proposed to be launched by the end of 2024 to a low-Earth orbit sun-synchronous orbit via rideshare for the 9-month mission.

We present the *Aspera* payload design and its expected performance, based on the design proposed to Pioneers AO, including partial updates made during the recent conceptual design study phase. This proceeding presents the scientific background (§2), an overview of payload (§3), the payload projected performance (§4), the science operation concept (§5), and our development plan (§6).

2. SCIENTIFIC BACKGROUND

2.1 Warm-hot Coronal Gas Halos and Galaxy Evolution

For over half a century, observational astrophysics has aspired to detect and map the most massive baryonic component of galaxies: the warm-hot coronal gas that is part of the CGM. Without observational constraints on properties of the warm-hot halo gas, galaxy evolution models are free to withdraw or deposit gas from the halo with impunity. Feedback balances the inflow and outflow of gas; therefore, measuring the state of a galaxy's gaseous halo constrains the other side of the galaxy evolution equation. Measurements of the coronal gas will constrain the detailed physics used in simulations, measure gas cooling rates,[8] gas recycling timescales, and the distances to which ionized galactic outflows can travel.[9] Emission from oxygen lines dominates radiative cooling for gas temperatures from 200,000–500,000 K,[8,10] allowing direct measurement of cooling rates for gas at halo virial temperatures. These cooling rates can be directly compared to the galaxy star formation rates to measure the fractional efficiency of turning gas into stars, which is a critical measure of feedback efficiency, and to cooling rates of gas at cooler temperatures to ensure overall consistency.[11]

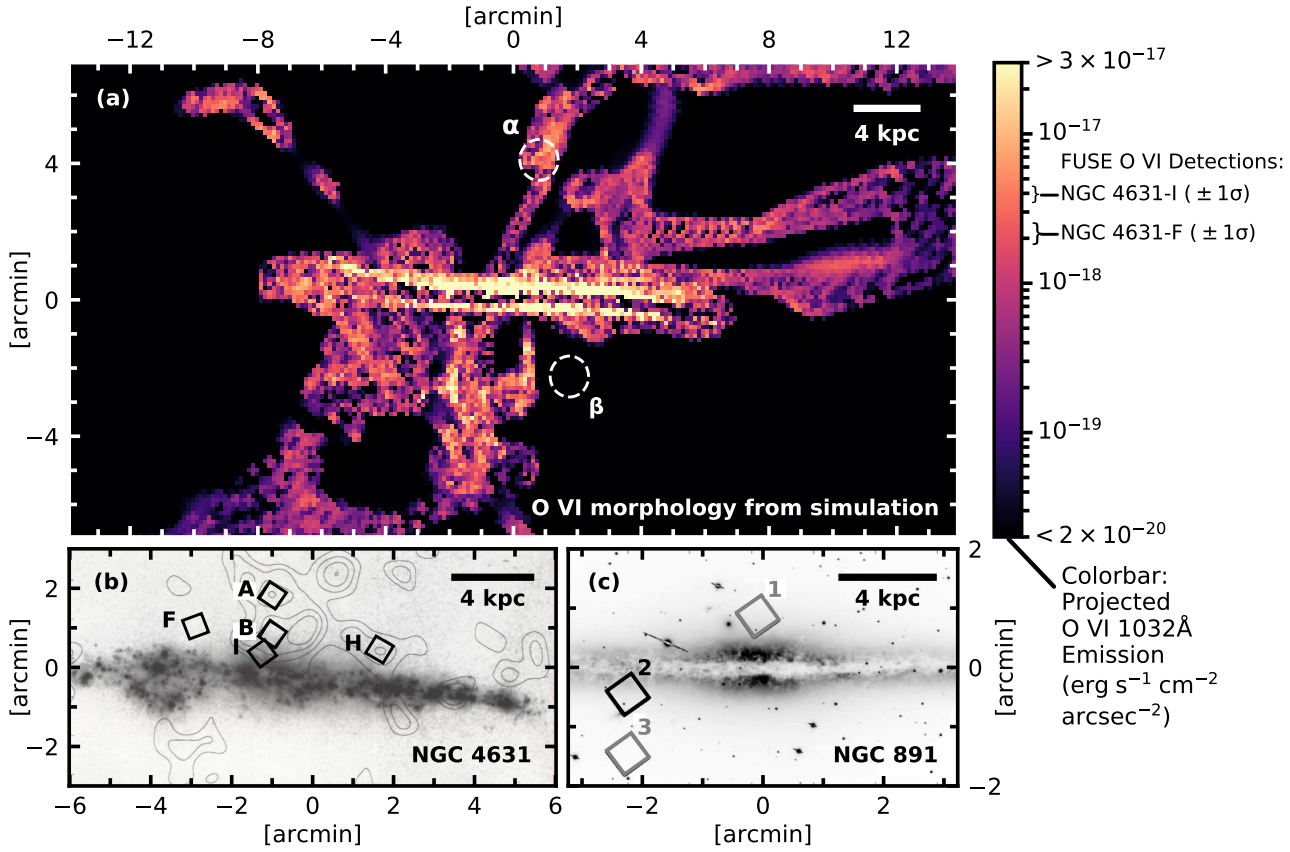

Figure 1: (a) Simulated O VI emission distribution from a MW-type galaxy at $z = 0$ based on simulations from a previous study,[4] provided in the edge-on perspective obtained in private communication with Corlies et al., positioned at 7.35 Mpc. Emission strength is scaled to match the O VI emission strength at around region α to the strength measured in the NGC 4631-B region.[5] The O VI detection from NGC 4631 can be explained if the pointings were made on a region similar to region α. In the same manner, O VI non-detections from NGC 891 pointings are aligned with the simulation result if they were made on pointings like region β. (b) $H\alpha$ image of NGC 4631, where X-ray contours are superposed, adopted and modified from Otte et al., 2003.[5] (c) BV image of NGC 891[6] adopted and modified from Otte et al., 2003.[5] O VI emissions are detected from all five fields in NGC 4631 (field A, B, F, H, I), and one field in NGC 891 (field 2),[5,7] marked with black squares. Two O VI non-detection fields (field 1, 3) are marked with grey squares.

Despite the importance of this gas to galaxy evolution, this phase remains unmapped. Morphological characteristics of the coronal gas phase, such as its extent, filling factor, and filamentary vs. cloud-like structures, are difficult to determine with pencil-beam absorption line studies.[12] Observations with *Aspera* will constrain the amount of halo gas, its cooling rate, recycling timescale, and the physical extent of ionized outflows—properties crucial to our understanding of galaxies and their evolution—for the first time.

2.2 Ubiquity of Warm-hot Gas and its Morphology

Due to the historical difficulty of measuring O VI emission, only a handful of studies have presented detections of coronal O VI emission lines, two in galaxy disks and one in the CGM.[5,13,14] These detections provide crucial empirical constraints that have informed our plan to map coronal gaseous halos. Otte et al.[5] provide the most directly relevant results for the objective of the *Aspera* mission. They searched for O VI emission beyond the disks of two nearby edge-on galaxies—NGC 4631 and NGC 891—using FUSE[15] spectra. They detected coronal gas in the two small observed fields (Field A and B, $30'' \times 30''$) in NGC 4631 and provided upper limits for fields in NGC 891 (See Figure 1). A re-examination of these data by the *Aspera* team was recently published, with

new O VI emission detections in NGC 4631 (Field F, I, H) and NGC 891 (Field 2), and upper limits for NGC 891.[7] Figure 1 shows the location of those O VI detection and non-detection fields in NGC 4631 and NGC 891.

The upper limits for O VI in NGC 891 are not surprising. Simulated O VI emission in galaxies and their halos shows an incredibly filamentary structure outside of the disk (Figure 1). It is possible that the fields chosen by Otte et al.[5] were unlucky and missed the O VI filaments in NGC 891. *Aspera* will confirm the filamentary structure predicted by simulations.

3. ASPERA PAYLOAD OVERVIEW

Aspera measures the O VI 1032 Å emission line using *four* parallel channels of modified Rowland-Circle configuration spectrographs, each with a 62 mm × 37 mm OAP primary mirror and a toroidal diffraction grating. *Aspera*'s spectrograph design is based on the heritage of FUSE and leverages the technological improvements that have been made since. A combination of conventional Lithium Fluoride coatings (LiF), improved quantum efficiency (QE) of micro-channel plate (MCP) detectors,[16] and low-scattering/high-efficiency holographic gratings[17] enables a system net throughput of 8.1%, which is 4.1× higher than FUSE. Each identical spectrograph channel is designed to have a moderate spectral resolving power (R ∼ 2000) at 1035 Å with a spatial resolution of 45″ (FWHM) over a 30′ slit length field of view (FoV). This parallel four-channel, four-slits configuration simplifies the assembly and engineering process while minimizing risk by eliminating a single point failure case. This configuration also allows *Aspera* to efficiently detect and map the 2D spatial distribution of O VI coronal gas over its short (9 months) mission lifetime using a "step-and-stare" observing strategy. All *Aspera* instrument systems, subsystems, and components are at a technology readiness level (TRL) 6+, including high heritage hardware (TRL 9) wherever possible. The system development benchmarks various similar Far-UV space telescopes run by NASA/ESA/JAXA in terms of wavelength range (1020-1050 Å) and optical design (Rowland-Circle). These benchmarks include FUSE, HST-COS, HISAKI,[18] and the *Alice* line of UV spectrographs for a variety of deep space missions, including Rosetta,[19] New Horizons,[20] LAMP,[21] and JUNO.[22]

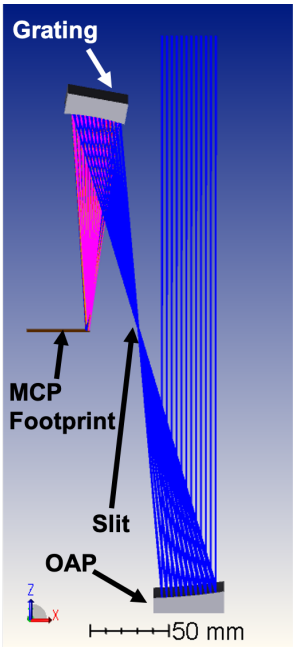

Figure 2: *Aspera* optics layout (one channel)

3.1 Optical Design: A SmallSat inspired by FUSE

The driving science requirements for the spectrograph optics are to obtain a spectral resolution of $\lambda/\delta\lambda > 1{,}500$ and spatial resolution $< 60''$ to resolve the O VI line emission, and distinguish its spatial distribution along the slit length direction. These requirements are met with the optical design in Figure 2. *Aspera*'s optical characteristics are shown in Table 1.

Parameter	Value
OAP primary mirror size (CA)	62 mm x 37 mm
OAP primary mirror RoC	342.4 mm
Plate scale at Slit	1205" mm^{-1}
Slit FoV (Length x Width)	60' x 30"
Toroidal grating size (CA)	64 mm x 34 mm
Toroidal grating RoC	138.8 mm, 149.8 mm
Grating line density	4800 lines mm^{-1}
Grating angle α, β at 103.4 nm	21.0°, 7.9°
Operating order	n = -1
Wavelength range	103.0 - 104.0 nm
Dispersion	1.392 nm mm^{-1}

Table 1: Optical characteristics of a single optics channel. OAP and grating sizes are clear aperture.

The *Aspera* design is slightly modified from the traditional Rowland-Circle configuration. The updated design has a flat and parallel detector plane among four channels, which enables two channels of optics to share one detector. This two-bounce design (primary mirror and grating) maximizes the overall throughput and has strong flight heritage. The design is also robust to contamination compared to more complex (# of bounces > 3) systems (less number of surfaces to be affected by the contamination). A 62 mm × 37 mm size (focal length: 171.2 mm) OAP primary maximizes the light collection power and provides optimum target spot size (< 21 μm RMS) over the wavelength and field ranges of interest. The combination of short focal length and the small spot size enables detector sampling limited spectral/spatial resolution, thus

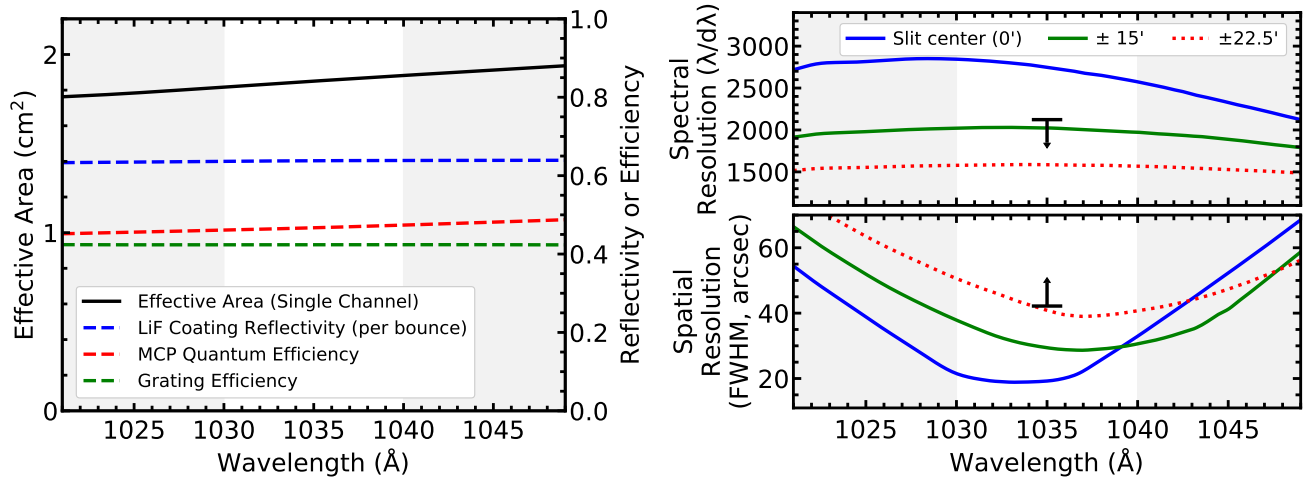

Figure 3: (Left) Effective area (single channel) and reflectivity/efficiency. (Right) Spectral and spatial resolution. Black arrows indicate the spectral/spatial resolution limited by the detector resolution.

effectively reducing the noise contribution from the detector background and stray/scattered light (Signal-limited sensitivity, §4).

Each four-channel primary mirror is identical, but they are aligned to look at slightly offset (60″) fields of view from each other on the sky, separated along the slit width direction (Figure 4). This arrayed four-channel system maximizes the 2D mapping capability and provides robust redundancy, such that the telescope can maintain 50–75% observing capability even after an unexpected critical performance degradation of a single-channel or detector failure. The optics are designed to place a spectrum footprint within 2 mm inside from the edge of the detector's active area where the optimal detector performance can be assured. The design of the telescope provides sufficient baffling to prevent straylight from objects outside the ±13° from the boresight. Additionally, a baffling scheme to minimize the stray and scattered light contribution from off-axis sources and non-operating grating orders is currently under development.

All optics will be coated with conventional Al+LiF coatings by Goddard Space Flight Center (GSFC). Initially, a recently developed "enhanced " Al+LiF coating (eLiF[23]), which has slightly higher reflectivity at (1035 Å), was considered. However, due to its low TRL (<6), eLiF was deemed too risky to implement into *Aspera*, making conventional Al+LiF the baseline coating for *Aspera* (which has TRL 9; e.g. FUSE).

An effective area curve of a single-channel spectrograph unit (Figure 3, left panel) is calculated by multiplying the light collecting area (62 mm × 37 mm), LiF coating reflectivity (two bounces),[23] MCP efficiency,[16] and the grating efficiency (from the simulation done by Horiba J-Y). The raytrace-driven spectral/spatial resolution estimation from a diffuse source is also presented in the right panel of Figure 3. Note that the actual resolutions are limited by the MCP resolution size, as indicated by black arrows. The line spread function (LSF) of a fully illuminated slit is presented in the right panel of Figure 7.

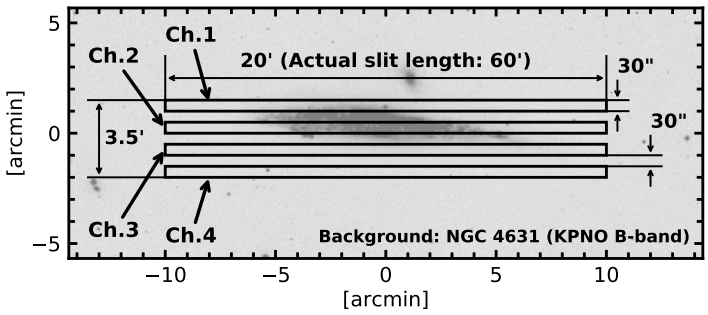

Figure 4: Slit array footprint of four offset channels on the sky. Note that the length of the actual slit (60′) is longer than the length (20′) in this figure.

The spectrograph slit is a conventional long slit with a 30″ × 60′ FoV that fulfills the mission requirement. It covers an extended spatial range (60′) beyond the required range (30′). The slit FoV of each spectrograph channel is offset by 1′ (slit center to center) side by side, as shown in Figure 4. Offset slits increase the detection

probability for spatially distributed O VI gas compared to overlapping slit FoVs. This offset will be achieved by a precise bore-sight alignment between each optics channel and the slit placement during the system assembly and integration process. The metering structure of the telescope maintains the alignment of the boresight of each channel with the star tracker. To characterize the variation of the boresight offsets, the characterization of the slit motion for each channel will be done during the thermo-vacuum and vibration testing. The offsets will also be measured on-board during the calibration period. The planned slit arrangement enables efficient 2D mapping of the O VI distribution in both step-and-stare or scan observation schemes.

Light reflecting off the OAP primary mirror is dispersed and focused by a 4,800-groove mm^{-1} toroidal grating. The current baseline grating will be holographically ruled by Horiba J-Y. The company has fabricated numerous high-groove-density gratings for various space missions, including the FUSE grating (5,300–5,800 grooves mm^{-1}).

3.2 Detector System

Aspera's four optical configurations are imaged using two cross delay line (XDL) MCP detectors. Each detector unit will be supplied by Sensor Sciences, LLC. Each MCP borosilicate micro-capillary array is coated with resistive and secondary emissive layers via atomic layer deposition (ALD), also a CsI photocathode achieves a detection QE of >40% at 1020–1050 Å.[16] The low intrinsic radioactivity of borosilicate glass plates allows for a lower background compared to the conventional lead glass plates (e.g., HST-COS). Additionally, these detectors are more resistant to gain sag issues because they use more stable secondary emissive layers made by atomic layer deposition.[16]

The proposed ALD-activated boroscillicate glass MCP detectors are similar to (but smaller than) the detectors baselined for LUVOIR-LUMOS and HabEx-UVS[24] and will be used for JUICE-UVS and Europa-UVS on-board ESA's JUICE mission (2022) and NASA's Europa Clipper mission (2024).[25,26] *Aspera*'s MCPs will be similar (in size, with a 40mm × 22 mm active area) to the detectors developed for the SPRITE cubesat, which is scheduled to be launched in 2022–2023.[26] To meet *Aspera*'s resolution requirements, each detector will be optimized to have ≤35-micron size resolution elements in both the spatial and spectral directions. The XDL detector electronics are at TRL 9 with heritage from the planetary science mission JUNO.

The expected QE of the detector in the *Aspera* bandpass is shown in Figure 3. The spectrum footprint on the detector covers an extended wavelength range (∼900 to 1080 Å), which is beyond the required range (1030 to 1040 Å) for *Aspera*; we note that the spatial/spectral resolution or sensitivity requirements for *Aspera*'s primary science objectives may not be satisfied at wavelengths outside the required range. The on-orbit detector background rate is expected to be <0.3 counts cm^{-2} s^{-1}, considering the low on-ground background rate and the small difference between the flight and ground background rate for a low mass satellite (∼60 kg).[27]

The detector is housed in a hermetically sealed vacuum enclosure with a LiF window. The sealed environment protects the reactive CsI photocathode from significant degradation in performance before launch of *Aspera*. The housing has vacuum/purge ports to either evacuate or purge (GN2) the detector during ground operations. The window, used for ground testing and calibration, is mounted on a spring-loaded door that can be deployed by a wax-pellet-type push actuator in orbit. Each detector package will have an independent readout electronics package (from Sensor Sciences, LLC) and a High Voltage Power Supply (HVPS). Based on prior implementations, each set of detector and electronics package has a mass of ∼1.2 kg (excluding ground support equipment and cables) and draws ∼6W of power (including the HVPS).

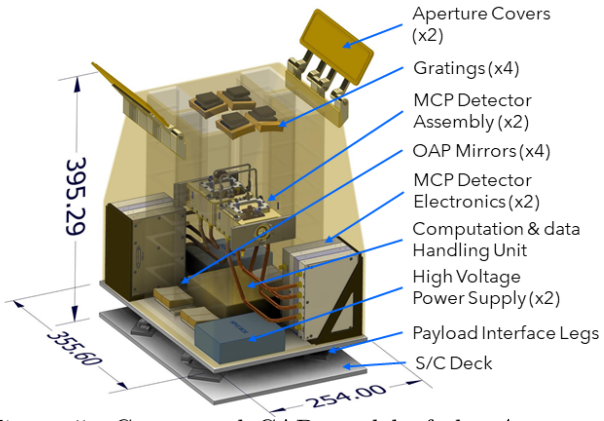

Figure 5: Conceptual CAD model of the *Aspera* payload assembly showing the internal configuration of key components. Dimensions are in mm.

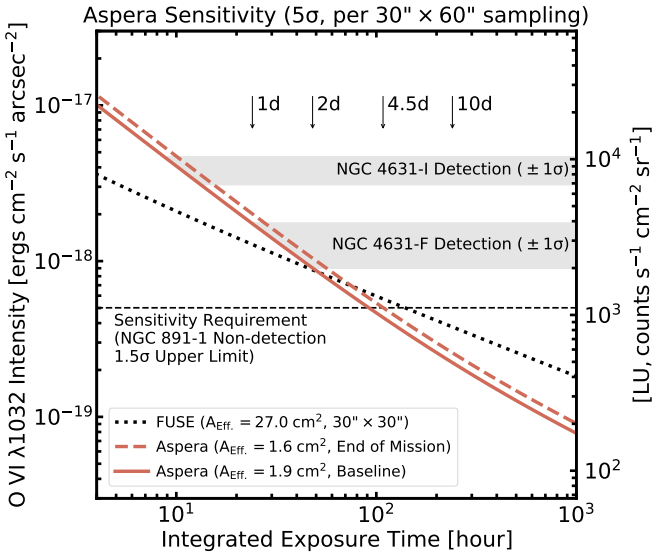

Parameter	*Aspera*	FUSE (Chung2021a)	Unit
Effective area	1.85	26.9	cm^2
Exposure time	388800	21536	sec
Target line intensity	**4.3E-19**	2.7E-18	erg s^{-1} cm^{-2} arcsec^{-2}
Target wavelength (typ.)	103.5		nm
Single photon energy (typ.)	1.92E-11		erg
Spatial sampling	60	30	arcsec
Slit width	30	30	arcsec
Total background rate at MCP	0.3	0.77	cts cm^{-2} s^{-1}
Spatial direction bin at MCP	0.0050	0.0800	cm
Spectral direction bin at MCP	0.0087	0.0960	cm
Total target signal	29	73	cts
Noise (MCP background)	2	11	cts
Noise (Total RSS)	6	14	cts
Total Signal to Noise Ratio	**5.0**	5.2	

Figure 6: (Left) *Aspera* single channel sensitivity. The solid red line is the expected sensitivity of *Aspera* vs. exposure time given the projected performance, while the dashed red line is the expected sensitivity at the end of 9-month mission assuming coating degradation (reflectivity loss of 7% per surface). The black dotted line is the estimated sensitivity of FUSE. (Right) S/N calculation breakdown of *Aspera*, compared to the case of O VI detection of NGC 4631-A from the FUSE mission.[7] The noise contribution from the MCP background is significantly smaller in *Aspera* vs. FUSE, due to the smaller size of detector area at given angular spatial sampling size.

3.3 Payload Structure

The *Aspera* instrument payload system is divided into the main optical subsystem and the supporting subsystems that interface with the spacecraft (S/C) bus. The opto-mechanical components (i.e., mirrors, gratings, and slits) and detectors for *Aspera* will be mounted on a metering structure to maintain the co-alignment of the channel slits on the sky and the internal alignment of each individual configuration. The individual optics will be mounted on the metering structure using isostatic three-point mounts that will be designed to survive mechanical stress during launch, minimize thermal deformation in orbit, and maintain the opto-mechanical alignment. The opto-mechanical tolerance and sensitivity analysis of the system indicates that the tolerance and alignment requirements for the system can be met with industry standard, heritage materials, and fabrication processes.

Figure 5 shows a top-level conceptual model of the payload that was used to generate a preliminary mass budget and to ensure that the payload can be accommodated by the spacecraft bus. The preliminary mass estimate for the payload is ∼24 kg and the estimated volume is within the payload volume constraint.

4. PROJECTED PAYLOAD PERFORMANCE

Aspera's sensitivity (Figure 6, left panel) is calculated for both nominal and marginal performance, considering the degradation of coating reflectivity over the 9-month mission lifetime.[28,29] The calculated sensitivity shows that the projected performance of *Aspera* satisfies the sensitivity requirement, even at the end of mission. The sensitivity metric for emission lines is expressed as the minimum detectable (Signal to noise ratio (S/N) ∼ 5) spectral line intensity per resolution element ($30'' \times 60''$) for a given exposure. Figure 6 shows that *Aspera*'s sensitivity is highly signal-limited, even at the very low surface line intensity level of $\sim 10^{-19}$ erg s^{-1} cm^{-2} arcsec^{-2}. This is because the most dominant source of noise is photon shot noise, and the other sources contribute considerably less to the total noise. The second dominant noise contribution is from the intrinsic detector background (1.0 counts day^{-1} resolution element^{-1}). Note that this background is significantly smaller than in the case of FUSE, due to the small detector binning area (4.1×10^{-5} cm^2) per resolution element. Other sources of noise

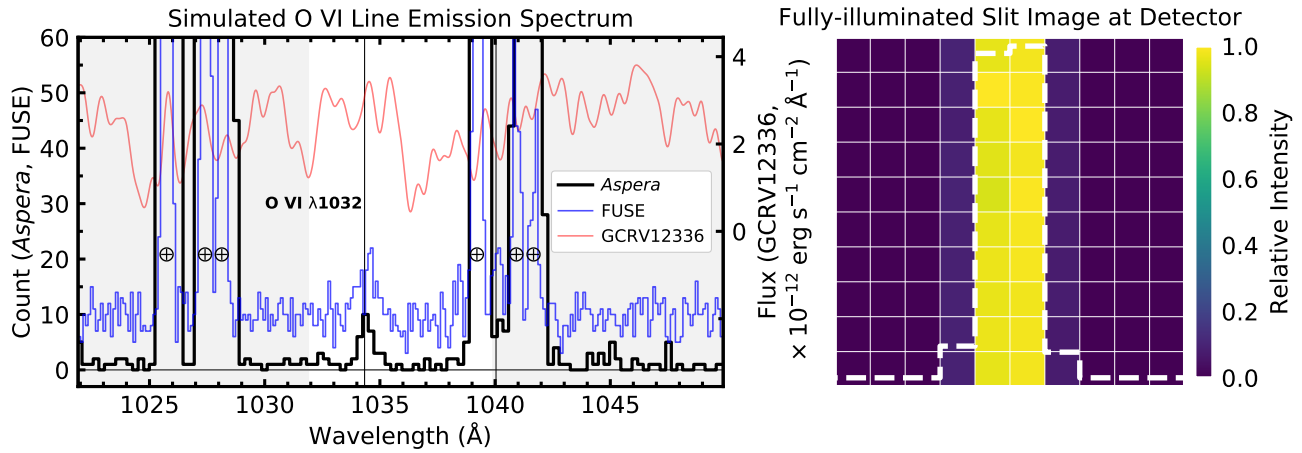

Figure 7: (Left, black) Simulated, LSF-convolved, random Poisson-noise-added 4.5-days exposure *Aspera* spectrum of O VI line emission, corresponding to intensity in Figure 6. (Blue) Reconstructed FUSE spectrum of O VI line detection from Otte et al.[32] (NGC 4631-A), again corresponding to the line intensity shown in Figure 6. (Red) *Aspera* LSF-convolved spectrum of GCRV12336, as a representative calibration target of *Aspera*. The locations of known geocoronal lines are marked with cross-circles. Two thin black vertical lines indicate O VI $\lambda\lambda$ 1032,1038 Å line locations. O VI lines are redshifted and broadened, assuming a 700 km s^{-1} line-of-sight recession velocity and a velocity dispersion of 200 km/s (FWHM). (Right) Image of a fully-illuminated slit at the detector (1034 Å). The dashed white line is an overlay of the histogram of the LSF.

are earthshine, zodiacal light, scattered light, and stray light. The known strength of earthshine (at 15° above from the Earth limb) and zodiacal light at ∼1050 Å is less than 0.2% of the *Aspera* sensitivity requirement.[30] The dominant source of scattered light is a geocoronal hydrogen Lyα line scattered by the grating, and its strength is estimated conservatively as < 0.01 counts day^{-1} resolution element^{-1}, from the low scattering property ($I/I_0 \sim 10^{-6}$) of the holographic grating.[31] Scattering from 0th and +1st order light will be controlled by an internal baffle/light trap, and the contribution from stray light is expected to be less than the detector intrinsic background with a light-tight opto-mechanical structure.

A representative S/N calculation breakdown is shown in the right panel of Figure 6. In the table, we compare the S/N calculation of *Aspera* and the known detection of O VI gas at NGC 4631-A from the FUSE observation by Chung et al.[7] as a reference. The known O VI detection S/N from Chung et al.[7] is well described by the photon shot noise and the total background noise. Spectral/spatial binning size of the FUSE detection is estimated from FUSE instrument parameters.[33] Note that the referenced FUSE background rate (0.77 counts cm^{-2} s^{-1}) is close to the lower end of the known range (0.6–2.0 counts cm^{-2} s^{-1}).[34] A simulated, random Poisson-noise-added *Aspera* spectrum corresponding to the representative S/N calculation (Figure 6) is shown in the left panel of Figure 7. The spectrum is convolved with the slit width and optics LSF. The *Aspera* LSF-convolved spectrum of GCRV12336, a central star of the planetary nebula M27, is also shown as a representative wavelength-calibration target.[34,35]

The predicted 2D S/N distribution of O VI 1032-Å gas mapped by *Aspera* is shown in Figure 8. The pixel size of the image is 30″ × 30″. The image is generated from the simulated O VI map of Milky Way-type galaxy, conservatively calibrated by matching the surface line intensity at around the filamentary structure (region α in Figure 1-(a) panel) to the known O VI intensity from the FUSE observation (NGC 4631-B pointing in Figure 1-(b) panel). The simulated galaxy is positioned at 7.35 Mpc, equal to the distance to NGC 4631;[36] thus it is spanned over 28′ × 14′ in angular space. The estimated net exposure time to obtain such a S/N distribution is 14 days in total, 2 days per pointing. The image includes the effects of S/C pointing uncertainty/jitter, slit broadening, and the field-dependent spectrograph point spread function. It shows that the expected 2D structure and the distribution of O VI gas can be resolved and mapped by *Aspera*.

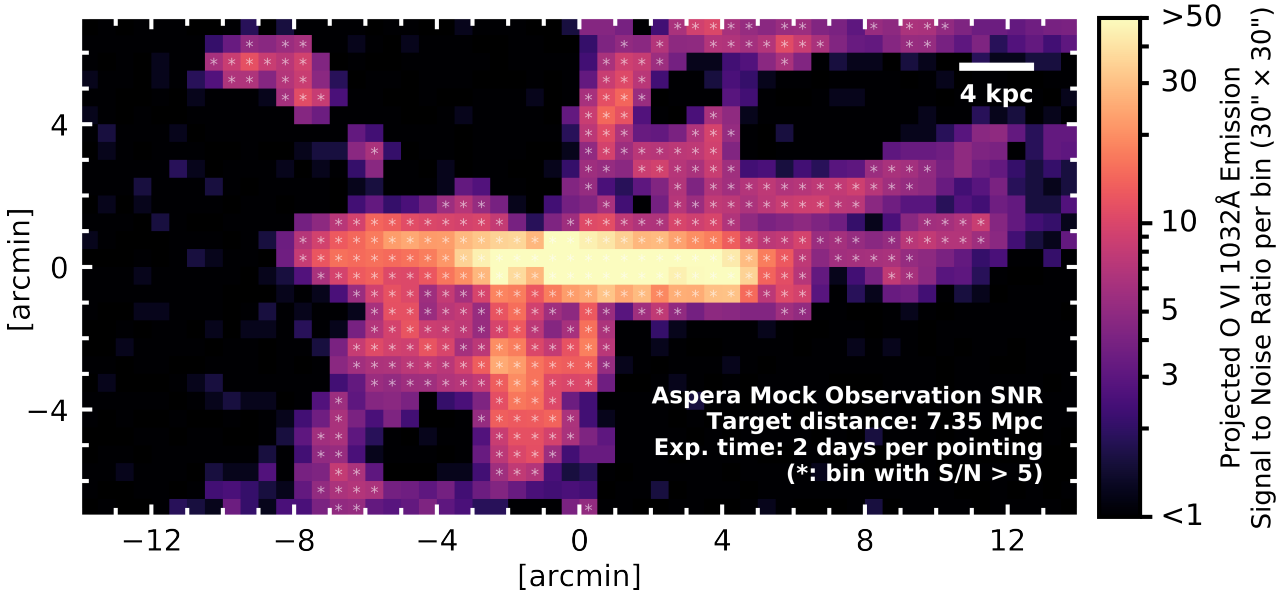

Figure 8: *Aspera* mock observation S/N distribution (random-noise effect included) derived from simulated O VI emission shown in Figure 1, run through *Aspera*'s projected system response, spacecraft pointing uncertainty/jitter, and optical aberration. The bin size is $30'' \times 30''$, and the bins with S/N > 5 are marked with asterisks. Seven pointings with a total exposure time of 14 days are required to completely map the $30' \times 14'$ region shown. Slices of the image are integrated over a shorter observing time and mosaiced.

5. SCIENCE OPERATION

The *Aspera* mission will focus on observing up to 10 nearby galaxy targets over its 9-month mission lifetime. Additional targets are in consideration if the mission duration is extended. The Sun-synchronous orbit (§5.1.1) for *Aspera* provides access to the full sky. The orbit also provides a constant, predictable environment that will stabilize the instrument performance, with limited and short eclipses.

5.1 Observing Strategy

During the first 5 months of science operation, *Aspera* will focus on O VI line emission "detection" by observing each target with a single pointing only, with pauses for re-visits to calibration sources and up/down links. A list of observing targets will be finalized at the time of mission operation (§5.1.2), although a tentative list of targets is shown here.

Each target will be observed for at least 4.5 days of exposure time to reach the sensitivity requirement level. If an O VI signal is detected in the galactic halo of a target, the next target will be observed. If the signal is not detected, the exposure will be extended up to 5.5 days or until O VI line emission is detected with S/N∼5, whichever comes first.

After the initial 5-month "discovery" phase, *Aspera* will spend the next 3 months re-visiting selected bright O VI emission-detected targets to 'map' the 2D distribution of O VI using a "step-and-stare" observing strategy. For each pointing in the

Name	RA (J2000)	Dec (J2000)	Priority Group	Optical Diameter (')	D (Mpc)	cz (km/s)
NGC 4631	12h42'8''	32°32'29''	1	17.0	7.4	606
NGC 3003	9h48'36''	33°25'17''	1	6.0	19.6	1478
M 82	9h55'53''	69°40'46''	1	13.0	4.2	203
NGC 5746	14h44'56''	1°57'18''	2	7.8	31.5	1724
NGC 1353	3h32'3''	-21°10'51''	2	5.2	25.6	1547
NGC 1569	4h30'49''	64°50'53''	3	5.8	3.4	-104
NGC 3692	11h28'24''	9°24'27''	3	3.6	42.4	1726
NGC 3044	9h53'41''	1°34'47''	3	5.0	21.4	1289
NGC 5775	14h53'58''	3°32'40''	3	4.4	17.4	1681
NGC 4666	12h45'9''	-1°32'17''	3	7.2	14.7	1529

Table 2: Representative list of *Aspera*'s science targets ordered by observing priority.

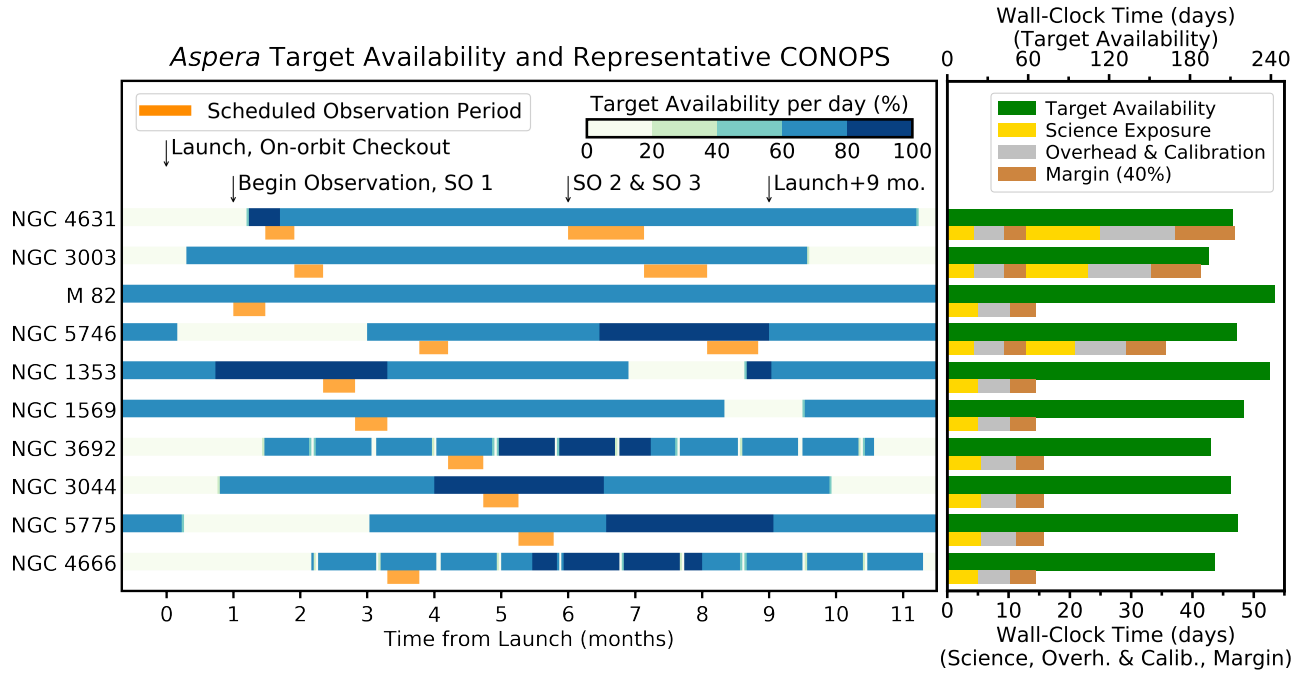

Figure 9: Availability of *Aspera* targets for one year and representative *Aspera* CONOPS.

"step-and-stare" strategy, we plan a total integration time of 2 days. The priority of mapping targets will be determined based on the strength of the detected O VI emission during the initial single pointing, target availability, and target galaxy characteristics.

5.1.1 Orbit

The preferred orbit for *Aspera* is a dawn-dusk Sun-synchronous orbit, which allows the S/C to operate in a benign power and stable thermal environment with minimal impact to scheduling. *Aspera* does not have strict constraints on orbital altitude, so any Sun-synchronous terminator orbit with altitude between 600 to 900 km (inclination: 97.8 – 99.0 deg) is acceptable. If possible, higher altitude (700 to 900 km, inclination: 98.2 – 99.0 deg) is preferred because that would reduce atmospheric drag, reduce orbital maintenance requirements to maintain a desired orbit, allow for greater mission longevity, and decrease the number of eclipses and the ratio of time spent in an eclipse. Also, the geocoronal line strength decreases with the orbit altitude.

For Concept of Operations (CONOPS), a modified PROBA 2 Sun-synchronous terminator orbit with an orbital altitude of 780 km (compared to a nominal 720 km in PROBA 2) is assumed. However, the exact orbit of *Aspera* depends strongly on the rideshare accommodations, which will be finalized later in the mission's development.

5.1.2 Observing CONOPS

Aspera's baseline 9-month mission is comprised of 1 month of orbit-checkout followed by 5 months dedicated to the primary mission campaign, and the remaining 3 months are dedicated to revisiting selected primary targets for mapping. This schedule can be revised in light of as-built performance and actual launch schedule. Assuming the modified PROBA 2 orbit (§5.1.1), the availability of 10 representative targets (Table 2) has been examined. Target accessibility is calculated from *Aspera*'s orbit, verifying that each target is not in a Sun, Earth, or Moon exclusion zone. Exclusion angles of 45, 15, and 10 degrees are used for the Sun, Earth limb, and the Moon.

Figure 9 shows the availability of representative targets for one year. Although the year-round availability of targets is diverse, the effective wall-clock availability is more than 180 days for all 10 targets. The figure also shows one of many possible observing scenarios for *Aspera*, according to the observing strategy (§5.1) and target availability, assuming a launch a date of Sep. 14, 2022 (for illustration only, not the planned launch date). This

CONOPS includes sufficient wall-clock time for general overhead (100% of science exposure time), calibration (6 hrs per target), and margin (40% of science exposure + overhead + calibration time).

In the event of a reduction of mission performance (i.e., failure of one detector or significant performance degradation of one or two sets of optics), the same CONOPS will be applied for the initial 5 months with less spatial coverage per target. For the later 3 months, 2 days of exposure per pointing will remain the same, but the number of pointings per target will be increased, such that the 2D mapping can be completed for at least 1 or 2 galaxies.

6. DEVELOPMENT PLAN

Aspera officially kicked off on April 1, 2021, and its Concept Study Report (CSR) will be submitted on September 1, 2021. The project then enters an aggressive Formulation period with a Preliminary Design Review (PDR) in late-June 2022 and Critical Design Review (CDR) in early-December 2022. The Implementation phase is a 32-month period that includes an engineering model build in 2023 and the flight model build completed in February 2024. The payload Test Readiness Review (TRR) is the gateway to a 3-month verification and validation effort concluding with the payload Pre-ship Review (PSR) in late-July 2024. Delivery to the spacecraft provider commences the payload/spacecraft integration and the final suite of environmental and systems tests. The Flight Readiness Review (FRR) is expected in Oct. 2024 with a nominal 1-month period between delivery to the launch partner and the launch date of November 29, 2024. Flight Ops. consists of a 1-month on-orbit checkout followed by an 8-month science observing program. End of mission is expected on September 5, 2025 with a project closeout at the end of January 2026, unless extended.

7. SUMMARY

Aspera was selected as one of the four inaugural 2020 NASA Astrophysics Pioneers program mission and is currently under development. The mission objective is to map the warm-hot phase gas (T$\sim$$10^5$ to 10^6K) in the halos of nearby galaxies for the first time. The payload design and its expected performance is presented here. The four-channel Rowland-circle-like EUV spectrographs on a single payload design was motivated by the FUSE mission. The simple but robust design of the *Aspera* payload provides a high-throughput system with redundancy even at the Small-Satellite space telescope level. The expected sensitivity of *Aspera* is 4.3×10^{-19} ergs/s/cm^2/arcsec^2 in 4.5 days of exposure time over four $60' \times 30''$ fields with $45''$ spatial resolution and R$\sim$2000 spectral resolution. The mission is currently in the conceptual design study phase, with the projected launch in late 2024 via a NASA-provided rideshare.

ACKNOWLEDGMENTS

This work is funded by NASA grant number 80NSSC21M0117 to the University of Arizona. This work is also supported by the University of Arizona's College of Science, Office of Research, Innovation, and Impact (ORII), the University of Arizona Space Institute (UASI), and the Department of Astronomy and Steward Observatory. Portions of this work were supported by the Arizona Board of Regents Technology Research Initiative Fund (TRIF). Keri Hoadley acknowledges support by the David & Ellen Lee Postdoctoral Fellowship in Experiment Physics at Caltech.

REFERENCES

[1] Tumlinson, J., Werk, J. K., Thom, C., Meiring, J. D., Prochaska, J. X., Tripp, T. M., O'Meara, J. M., Okrochkov, M., and Sembach, K. R., "Multiphase Gas in Galaxy Halos: The O VI Lyman-limit System toward J1009+0713," *ApJ* **733**, 111 (Jun 2011).

[2] Tumlinson, J., Thom, C., Werk, J. K., Prochaska, J. X., Tripp, T. M., Katz, N., Davé, R., Oppenheimer, B. D., Meiring, J. D., Ford, A. B., O'Meara, J. M., Peeples, M. S., Sembach, K. R., and Weinberg, D. H., "The COS-Halos Survey: Rationale, Design, and a Census of Circumgalactic Neutral Hydrogen," *ApJ* **777**, 59 (Nov 2013).

[3] Tumlinson, J., Peeples, M. S., and Werk, J. K., "The Circumgalactic Medium," *ARA&A* **55**, 389–432 (Aug 2017).

[4] Corlies, L. and Schiminovich, D., "Empirically Constrained Predictions for Metal-line Emission from the Circumgalactic Medium," *ApJ* **827**, 148 (Aug 2016).

[5] Otte, B., Murphy, E. M., Howk, J. C., Wang, Q. D., Oegerle, W. R., and Sembach, K. R., "Probing O VI Emission in the Halos of Edge-on Spiral Galaxies," *ApJ* **591**, 821–826 (Jul 2003).

[6] Howk, J. C. and Savage, B. D., "The Multiphase Halo of NGC 891: WIYN Hα and BVI Imaging," *AJ* **119**, 644–667 (Feb 2000).

[7] Chung, H., Vargas, C. J., and Hamden, E., "Revisiting FUSE o vi emission in galaxy halos," *The Astrophysical Journal* **916**, 7 (jul 2021).

[8] Ferland, G. J., Chatzikos, M., Guzmán, F., Lykins, M. L., van Hoof, P. A. M., Williams, R. J. R., Abel, N. P., Badnell, N. R., Keenan, F. P., Porter, R. L., and Stancil, P. C., "The 2017 Release Cloudy," *Revista Mexicana de Astronomia y Astrofisica* **53**, 385–438 (Oct 2017).

[9] Rupke, D. S. N., Coil, A., Geach, J. E., Tremonti, C., Diamond-Stanic, A. M., George, E. R., Hickox, R. C., Kepley, A. A., Leung, G., Moustakas, J., Rudnick, G., and Sell, P. H., "A 100-kiloparsec wind feeding the circumgalactic medium of a massive compact galaxy," *Nature* **574**, 643–646 (Oct 2019).

[10] Schure, K. M., Kosenko, D., Kaastra, J. S., Keppens, R., and Vink, J., "A new radiative cooling curve based on an up-to-date plasma emission code," *A&A* **508**, 751–757 (Dec 2009).

[11] Zhang, H., Zaritsky, D., Pardos Olsen, K., Behroozi, P., Werk, J., Kennicutt, R., Xie, L., Yang, X., Fang, T., De Lucia, G., Hirschmann, M., and Fontanot, F., "An Empirical Determination of the Dependence of the Circumgalactic Mass Cooling Rate and Feedback Mass Loading Factor on Galactic Stellar Mass," *arXiv e-prints* , arXiv:2104.12777 (Apr. 2021).

[12] Werk, J. K., Prochaska, J. X., Cantalupo, S., Fox, A. J., Oppenheimer, B., Tumlinson, J., Tripp, T. M., Lehner, N., and McQuinn, M., "The COS-Halos Survey: Origins of the Highly Ionized Circumgalactic Medium of Star-Forming Galaxies," *ApJ* **833**, 54 (Dec 2016).

[13] Grimes, J. P., Heckman, T., Strickland, D., Dixon, W. V., Sembach, K., Overzier, R., Hoopes, C., Aloisi, A., and Ptak, A., "Feedback in the Local Lyman-break Galaxy Analog Haro 11 as Probed by Far-Ultraviolet and X-Ray Observations," *ApJ* **668**, 891–905 (Oct 2007).

[14] Hayes, M., Melinder, J., Östlin, G., Scarlata, C., Lehnert, M. D., and Mannerström-Jansson, G., "O VI Emission Imaging of a Galaxy with the Hubble Space Telescope: a Warm Gas Halo Surrounding the Intense Starburst SDSS J115630.63+500822.1," *ApJ* **828**, 49 (Sep 2016).

[15] Moos, H. W., Cash, W. C., Cowie, L. L., Davidsen, A. F., Dupree, A. K., Feldman, P. D., Friedman, S. D., Green, J. C., Green, R. F., Gry, C., Hutchings, J. B., Jenkins, E. B., Linsky, J. L., Malina, R. F., Michalitsianos, A. G., Savage, B. D., Shull, J. M., Siegmund, O. H. W., Snow, T. P., Sonneborn, G., Vidal-Madjar, A., Willis, A. J., Woodgate, B. E., York, D. G., Ake, T. B., Andersson, B. G., Andrews, J. P., Barkhouser, R. H., Bianchi, L., Blair, W. P., Brownsberger, K. R., Cha, A. N., Chayer, P., Conard, S. J., Fullerton, A. W., Gaines, G. A., Grange, R., Gummin, M. A., Hebrard, G., Kriss, G. A., Kruk, J. W., Mark, D., McCarthy, D. K., Morbey, C. L., Murowinski, R., Murphy, E. M., Oegerle, W. R., Ohl, R. G., Oliveira, C., Osterman, S. N., Sahnow, D. J., Saisse, M., Sembach, K. R., Weaver, H. A., Welsh, B. Y., Wilkinson, E., and Zheng, W., "Overview of the Far Ultraviolet Spectroscopic Explorer Mission," *ApJL* **538**, L1–L6 (July 2000).

[16] Siegmund, O. H. W., Vallerga, J. V., Darling, N., Curtis, T., McPhate, J., Hull, J. S., Cremer, T., Ertley, C., Foley, M., Minot, M., Graves, G., Paw U, C., and Vo, C., "UV imaging detectors with high performance microchannel plates," in [*UV, X-Ray, and Gamma-Ray Space Instrumentation for Astronomy XXI*], *Society of Photo-Optical Instrumentation Engineers (SPIE) Conference Series* **11118**, 111180N (Sept. 2019).

[17] Cotel, A., Liard, A., Desserouer, F., and Pichon, P., "Overview of diffraction gratings technologies for spaceflight satellites and ground-based telescopes," in [*International Conference on Space Optics — ICSO 2014*], Sodnik, Z., Cugny, B., and Karafolas, N., eds., **10563**, 194 – 201, International Society for Optics and Photonics, SPIE (2017).

[18] Yoshioka, K., Murakami, G., Yamazaki, A., Tsuchiya, F., Kagitani, M., Sakanoi, T., Kimura, T., Uemizu, K., Uji, K., and Yoshikawa, I., "The extreme ultraviolet spectroscope for planetary science, EXCEED," *Planet. Space Sci.* **85**, 250–260 (Sept. 2013).

[19] Stern, S. A., Slater, D. C., Scherrer, J., Stone, J., Versteeg, M., A'Hearn, M. F., Bertaux, J. L., Feldman, P. D., Festou, M. C., Parker, J. W., and Siegmund, O. H., "Alice: The rosetta ultraviolet imaging spectrograph," *Space Science Reviews* **128**(1-4), 507–527 (2007).

[20] Stern, S. A., Scherrer, J., Slater, D. C., Gladstone, G. R., Dirks, G., Stone, J., Davis, M., Versteeg, M., and Siegmund, O. H. W., "ALICE: the ultraviolet imaging spectrograph aboard the New Horizons Pluto mission spacecraft," in [*Astrobiology and Planetary Missions*], Hoover, R. B., Levin, G. V., Rozanov, A. Y., and Gladstone, G. R., eds., **5906**, 358 – 367, International Society for Optics and Photonics, SPIE (2005).

[21] Davis, M. W., Gladstone, G. R., Versteeg, M. H., Greathouse, T. K., Stern, S. A., Parker, J. W., Steffl, A. J., Retherford, K. D., and Slater, D. C., "Commissioning and in-flight calibration results of the Lunar Reconnaissance Orbiter's Lyman Alpha Mapping Project (LRO/LAMP) UV imaging spectrograph," in [*UV/Optical/IR Space Telescopes and Instruments: Innovative Technologies and Concepts V*], MacEwen, H. A. and Breckinridge, J. B., eds., **8146**, 33 – 41, International Society for Optics and Photonics, SPIE (2011).

[22] Gladstone, G. R., Persyn, S. C., Eterno, J. S., Walther, B. C., Slater, D. C., Davis, M. W., Versteeg, M. H., Persson, K. B., Young, M. K., Dirks, G. J., Sawka, A. O., Tumlinson, J., Sykes, H., Beshears, J., Rhoad, C. L., Cravens, J. P., Winters, G. S., Klar, R. A., Lockhart, W., Piepgrass, B. M., Greathouse, T. K., Trantham, B. J., Wilcox, P. M., Jackson, M. W., Siegmund, O. H. W., Vallerga, J. V., Raffanti, R., Martin, A., Gérard, J.-C., Grodent, D. C., Bonfond, B., Marquet, B., and Denis, F., "The ultraviolet spectrograph on nasa's juno mission," *Space Science Reviews* **213**, 447–473 (Nov 2017).

[23] Quijada, M. A., Boris, D. R., del Hoyo, J., Wollack, E. J., Kozen, A. C., Walton, S., and Dwivedi, V., "E-beam generated plasma etching for developing high-reflectance mirrors for far-ultraviolet astronomical instrument applications," in [*Proceedings of the SPIE*], *Society of Photo-Optical Instrumentation Engineers (SPIE) Conference Series* **10699**, 106992X (Jul 2018).

[24] Siegmund, O. H. W., Ertley, C., Vallerga, J. V., Schindhelm, E. R., Harwit, A., Fleming, B. T., France, K. C., Green, J. C., McCandliss, S. R., and Harris, W. M., "Microchannel plate detector technology potential for LUVOIR and HabEx," in [*UV, X-Ray, and Gamma-Ray Space Instrumentation for Astronomy XX*], Siegmund, O. H., ed., **10397**, 282 – 295, International Society for Optics and Photonics, SPIE (2017).

[25] Davis, M. W., Siegmund, O. H. W., Gladstone, G. R., Martin, A., Molyneux, P. M., Retherford, K. D., Veach, T. J., and Vallerga, J. V., "Bench and thermal vacuum testing of the JUICE-UVS microchannel plate detector system," in [*UV, X-Ray, and Gamma-Ray Space Instrumentation for Astronomy XXI*], Siegmund, O. H., ed., **11118**, 214 – 224, International Society for Optics and Photonics, SPIE (2019).

[26] Fleming, B. T., France, K., Williams, J., Ulrich, S., Tumlinson, J., McCandliss, S., O'Meara, J., Sankrit, R., Borthakur, S., Jaskot, A., Rutkowski, M., Quijada, M., Hennessy, J., and Siegmund, O., "High-sensitivity far-ultraviolet imaging spectroscopy with the SPRITE Cubesat," in [*UV, X-Ray, and Gamma-Ray Space Instrumentation for Astronomy XXI*], *Society of Photo-Optical Instrumentation Engineers (SPIE) Conference Series* **11118**, 111180U (Sept. 2019).

[27] Siegmund, O. H. W., McPhate, J. B., Curtis, T., Darling, N., Vallerga, J. V., Cremer, T., and Ertley, C., "Development of UV imaging detectors with atomic layer deposited microchannel plates and cross strip readouts," in [*Society of Photo-Optical Instrumentation Engineers (SPIE) Conference Series*], *Society of Photo-Optical Instrumentation Engineers (SPIE) Conference Series* **11454**, 114541H (Dec. 2020).

[28] Oliveira, C. M., Retherford, K., Conard, S. J., Barkhouser, R. H., and Friedman, S. D., "Aging studies of LiF-coated optics for use in the far ultraviolet," in [*EUV, X-Ray, and Gamma-Ray Instrumentation for Astronomy X*], Siegmund, O. H. and Flanagan, K. A., eds., *Society of Photo-Optical Instrumentation Engineers (SPIE) Conference Series* **3765**, 52–60 (Oct. 1999).

[29] Fleming, B., Quijada, M., Hennessy, J., Egan, A., Hoyo, J. D., Hicks, B. A., Wiley, J., Kruczek, N., Erickson, N., and France, K., "Advanced environmentally resistant lithium fluoride mirror coatings for the next generation of broadband space observatories," *Appl. Opt.* **56**, 9941–9950 (Dec 2017).

[30] Dashtamirova, D., Fischer, W. J., and et al., [*Cosmic Origins Spectrograph Instrument Handbook, Version 12.1*] (2020).

[31] Woods, T. N., Wrigley, R. T., Rottman, G. J., and Haring, R. E., "Scattered-light properties of diffraction gratings," *Appl. Opt.* **33**, 4273–4285 (Jul 1994).

[32] Otte, B., Dixon, W. V., and Sankrit, R., "The Far Ultraviolet Spectroscopic Explorer Detection of Galactic O VI Emission in the Halo above the Perseus Arm," *ApJL* **586**, L53–L56 (Mar. 2003).

[33] Kaiser, M. E. and Kruk, J. W., [*FUSE Instrument Handbook, June 16, 2009 Edition*] (2009).

[34] Dixon, W. V., Sahnow, D. J., Barrett, P. E., Civeit, T., Dupuis, J., Fullerton, A. W., Godard, B., Hsu, J. C., Kaiser, M. E., Kruk, J. W., Lacour, S., Lindler, D. J., Massa, D., Robinson, R. D., Romelfanger, M. L., and Sonnentrucker, P., "CalFUSE Version 3: A Data Reduction Pipeline for the Far Ultraviolet Spectroscopic Explorer," *PASP* **119**, 527–555 (May 2007).

[35] McCandliss, S. R., France, K., Lupu, R. E., Burgh, E. B., Sembach, K., Kruk, J., Andersson, B. G., and Feldman, P. D., "Molecular and Atomic Excitation Stratification in the Outflow of the Planetary Nebula M27," *ApJ* **659**, 1291–1316 (Apr. 2007).

[36] Tully, R. B., Courtois, H. M., Dolphin, A. E., Fisher, J. R., Héraudeau, P., Jacobs, B. A., Karachentsev, I. D., Makarov, D., Makarova, L., Mitronova, S., Rizzi, L., Shaya, E. J., Sorce, J. G., and Wu, P.-F., "Cosmicflows-2: The Data," *AJ* **146**, 86 (Oct. 2013).